Journal of Anatomy

J. Anat. (2013) **222**, pp214–222 doi: 10.1111/joa.12005

Intramuscular architecture of the autochthonous back muscles in humans

Heiko Stark,[1,2] Rosemarie Fröber[3] and Nadja Schilling[1,4]

[1]*Institute of Systematic Zoology and Evolutionary Biology, Friedrich-Schiller-University, Jena, Germany*
[2]*Department of Bioinformatics, Friedrich-Schiller-University, Jena, Germany*
[3]*Institute of Anatomy I, Jena University Hospital, Jena, Germany*
[4]*Small Animal Clinic, University of Veterinary Medicine Hannover, Hannover, Germany*

Abstract

Many training concepts take muscle properties such as contraction speed or muscle topography into account to achieve an optimal training outcome. Thus far, the internal architecture of muscles has largely been neglected, although it is well known that parameters such as pennation angles or the lengths of fascicles but also the proportions of fleshy and tendinous fascicle parts have a major impact on the contraction behaviour of a muscle. Here, we present the most detailed description of the intramuscular fascicle architecture of the human perivertebral muscles available so far. For this, one adult male cadaver was studied. Our general approach was to digitize the geometry of each fascicle of the muscles of back proper (Erector spinae) – the Spinalis thoracis, Iliocostalis lumborum, Longissimus thoracis and the Multifidus thoracis et lumborum – and of the deep muscles of the abdomen – Psoas minor, Psoas major and Quadratus lumborum – during a layerwise dissection. Architectural parameters such as fascicle angles to the sagittal and the frontal planes as well as fascicle lengths were determined for each fascicle, and are discussed regarding their consequences for the function of the muscle. For example, compared with the other dorsovertebral muscles, the Longissimus thoracis can produce greater shortening distances because of its relatively long fleshy portions, and it can store more elastic energy due to both its relatively long fleshy and tendinous fascicle portions. The Quadratus lumborum was outstanding because of its many architectural subunits defined by distinct attachment sites and fascicle lengths. The presented database will improve biomechanical models of the human trunk by allowing the incorporation of anisotropic muscle properties such as the fascicle direction into finite element models. This information will help to increase our understanding of the functionality of the human back musculature, and may thereby improve future training concepts.

Key words: epaxial; fascicle angle; fibre bundle; hypaxial; skeletal muscle.

Introduction

Various training concepts in preventive and rehabilitative medicine take muscle properties such as contraction speed (fast vs. slow) or the topography of the muscles (mono- or biarticular) into account to achieve an optimal training outcome. Thus far, the internal architecture of muscles has largely been ignored, although it is well known that parameters such as pennation angles or the lengths of muscle fascicles, as well as the proportions of fleshy to tendinous fascicle parts have a major impact on the contraction behaviour of a muscle. Based on the fascicle arrangement, pennated and non-pennated muscles are distinguished. This distinction is crucial for a muscle's force exertion because the fascicles transmit force to the tendon and/or bone at different angles. The length and the pennation angle of the fascicles specify the velocity, distance and the force exerted during a muscle's contraction. In general, pennated muscles are well suited to exert high forces over short contraction distances, while a non-pennate architecture is well suited for high contraction velocities and distances (Benninghoff & Rollhäuser, 1952; Gans & Bock, 1965; Langenberg, 1970). Considering these architectural specifications in the design of rehabilitation, training and exercise programmes may help to improve their outcome.

To estimate contraction parameters such as force or velocity, usually the superficial fascicle orientation is used, although several studies have shown that the internal architecture cannot necessarily be inferred from the

Correspondence
Heiko Stark, Lehrstuhl für Bioinformatik, Friedrich-Schiller-Universität Jena, Ernst-Abbe-Platz 2, 07737 Jena, Germany. T: ++ 49 3641 949584; F: ++ 49 3641 946452; E: heiko@starkrats.de

Accepted for publication *1 October 2012*
Article published online *4 November 2012*

superficial arrangement (Benninghoff & Rollhäuser, 1952; Gans, 1982; Sacks & Roy, 1982; Paul, 2001; Stark & Schilling, 2010). In many cases, the internal fascicle orientation is much more complex, for example, due to so-called 'intramuscular inhomogeneities' (i.e. local differences in fascicle pennation and length). Within the last few decades, mathematical modelling has developed tremendously, so much so that currently, the internal architecture of a muscle can also be simulated and evaluated (Lemos et al. 2004, 2005; Blemker & Delp, 2005, 2006). In doing so, individual finite elements representing the contractile subunits are linked by mathematical equations. This approach takes the inner architecture into account via vector fields, and as a result considers local differences of fascicle pennation (anisotropy). Additionally, volume shifts or the ratio of tendinous to fleshy fascicle parts can be included. The resulting simulations are increasingly detailed and new questions can be addressed such as: 'What influence do volume shifts have on adjacent muscles?' or 'How does the sarcomere length change during a contraction?' Furthermore, it is possible to integrate different muscle properties, for example, different fibre types, and thus to simulate dynamic processes such as fatigue behaviour.

Compared with limb muscles, the perivertebral musculature is rather complex due to its many layers of muscles, comprising fibre bundles of various lengths and orientations. Possibly related to this, how to train these architecturally diverse muscles has been under debate for decades (Jellema et al. 2001; Linton & Tulder, 2001; Barr et al. 2005, 2007; van Tulder et al. 2006; Chou et al. 2007). Additionally, the internal architecture is crucial in identifying local maxima in stress and strain distribution during a contraction, which may relate to the aetiology of back pain. A better understanding of the intramuscular architecture and its role may help to improve surgical approaches and preserve the postoperative function of the muscles. Addressing such problems is currently hampered by our limited knowledge on the intramuscular architecture of the perivertebral musculature. With the exception of Dumas et al. (1988, 1991), who measured the curvilinear architecture of trunk muscles, only the origins and insertions of the fascicles or muscles were considered in previous studies, and therefore details on the exact fascicle geometry were not included (Macintosh & Bogduk, 1991; Bogduk et al. 1992a,b; Han et al. 1992; Stokes & Gardner-Morse, 1999; Poelstra et al. 2000).

With this 3D reconstruction of the autochthonous back muscles, we aim at increasing our knowledge and understanding of intramuscular architecture of the human back musculature, in order to allow for the incorporation of these properties in future training concepts and biomechanical modelling. Our general approach was to digitize the geometry of each fascicle of the perivertebral musculature during layerwise dissection.

Materials and methods

Cadaver, bone and muscle processing

One embalmed adult male cadaver [57 years old, 1.72 m, 92.6 kg, body mass index (BMI) 31.3 kg m^{-2}] was studied. The donor had no degenerative diseases of the musculoskeletal system and the cause of death was bronchial carcinoma. The study was approved by the ethics committee of the University Hospital Jena, Germany (3087-03/11).

Prior to the dissection and 3D reconstruction, the complete torso was CT-scanned and the skeleton was reconstructed from the image stack using 'ImageJ' (http://rsbweb.nih.gov/ij/) and 'Imaris' (http://www.bitplane.com/). The Dicom-images (512 × 512 pixels, 16-bit grey value depth) were converted into Tiff-images using 'Dicom2' (http://barre.nom.fr/medical/dicom2/). Afterwards, the Tiff-image stack was loaded into 'ImageJ' to segment the skeletal structures and separate them from the surrounding tissue. For this, the grey-scale threshold was adjusted repeatedly, while processing the image stack, to allow for the separate reconstruction of each bone (Fig. 1c). In result, a separate image stack represented each bone. The skeletal elements were then reconstructed in 'Imaris' and saved as 3D objects (Fig. 1a,b).

After removal of the skin and the subcutaneous fat, the superficial back muscles – Trapezius, Latissimus dorsi, Serratus posterior inferior muscles – were removed. Titan screws were placed on palpable skeletal landmarks along the spine and iliac blades of the pelvis, which allowed for the monitoring of potential bone movements during the dissection and served as a reference system for the 3D reconstruction (Fig. 1). For the reconstruction, a dorsal and a ventral reference system was established because the ventral markers were not accessible during the dissection of the dorsovertebral musculature and vice versa (Fig. 1d, red and blue). These two reference systems were linked to each other using overlapping lateral landmarks (Fig. 1d, green). The relative movements of the markers during the dissection are shown in Fig. 1d (top). The mean relative motion was 0.14 ± 0.08 mm for the dorsal and 0.44 ± 0.51 mm for the ventral markers (mean ± SD; Fig. 1d). The ventral relative motion was somewhat higher because of greater instability of the torso after the removal of the dorsal muscles and the abdominal wall. A global coordinate system based on Wu & Cavanagh (1995) and Wu et al. (2002) was established to align all data relative to the global origin, which was set at the mid-point between adjacent endplates of the last thoracic vertebra with the *X*-axis pointing ventrally, the *Y*-axis cranially and the *Z*-axis pointing to the right side of the body.

To reconstruct the fascicles, 3D coordinates of several data points along each fascicle were measured using the 3D digitizer 'Microscribe' (http://www.immersion.com/), while the muscles were dissected layerwise on both sides of the body (similar to Dumas et al. 1988, 1991; van Eijden et al. 1996; Poelstra et al. 2000; Kim et al. 2007; Rosatelli et al. 2008). Additionally, 3D coordinates at the beginning and the end of the fleshy and the tendinous parts, and of each fascicle's origin and insertion were collected. These data were stored on a computer for further processing. To prevent drying, the body was kept moist and covered with damp cloths.

Of the proper back muscles (Erector spinae; Federative Committee on Anatomical Terminology, 1998), only the largest ones – the Spinalis thoracis (SP in Data S1), Iliocostalis lumborum (ILC in Data S2), Longissimus thoracis (LG in Data S3) and the Multifidus thoracis

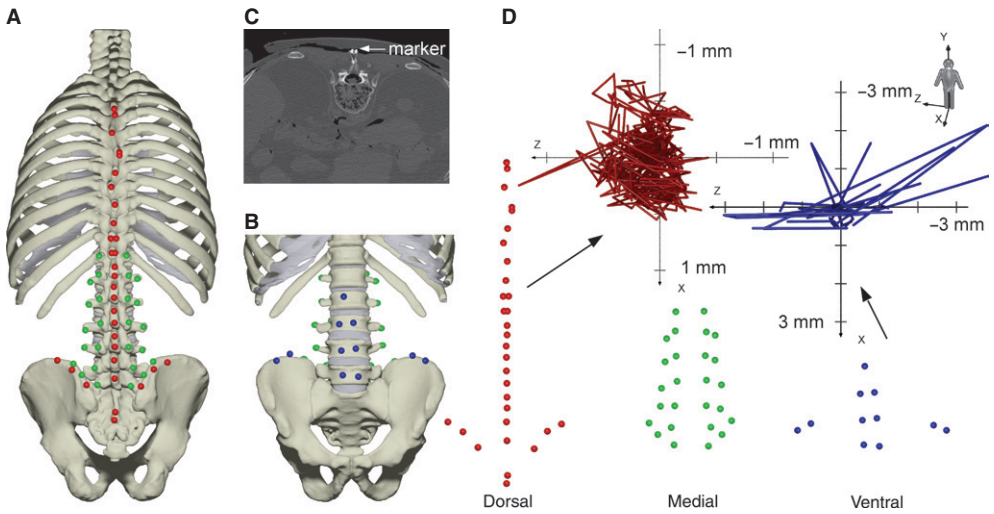

Fig. 1 3D reconstruction of the spine, ribs and pelvis of the studied cadaver in (a) dorsal and (b) ventral perspectives. The dorsal skeletal markers are shown in red, the ventral ones are shown in blue. The overlapping lateral markers are in green (for details, see Materials and methods). (c) Example of an image from the CT image stack used to reconstruct the skeletal elements. Note the titan screws in the dorsal spine, which served as reference markers during the dissection. (d) Relative movements of the dorsal (red) and the ventral (blue) markers in the mediolateral (*z*) and the dorsoventral (*x*) directions, which occurred between sessions of data collection. Each data point reflects one recording day. Note the relatively small movements during the dorsal dissection, compared with the movements during the ventral dissection. The green markers, which are visible in prone and supine positions of the specimen, were used to align the dorsal and ventral reference systems.

et lumborum (M in Data S4) – will be presented in this study. Part of the dissection of these muscles on the left side of the body served to establish the protocol for the data collection, which is why tendinous parts of some fascicles are missing. However, a complete dataset was collected from the right side of the body. In total, geometrical data of 687 fleshy (369 left, 318 right) and 204 tendinous fascicle parts (only the right side) were recorded for the four muscles of the proper back. After finishing the data collection on the dorsal aspect of the spine, the cadaver was turned. The skin and the subcutaneous fat from the abdominal wall and the muscles of the abdomen – Rectus abdominis, Pyramidalis, External oblique, Internal oblique and Transversus abdominis muscles – as well as the abdominal viscera were removed. The deep muscles of the abdomen on the ventral aspect of the spine – Psoas minor (PMN in Data S6), Psoas major (PMJ in Data S5) and Quadratus lumborum (Q in Data S7) muscles – were dissected. Altogether, 406 fleshy (230 left, 176 right) and 251 tendinous fascicle parts (147 left, 104 right) were digitized ventrally.

3D reconstruction and data analysis

The data collected were further processed by removing certain artefacts and aligning the muscles relative to the skeleton using a custom-made software 'Cloud2' (http://starkrats.de). To compare between body sides, the datasets were first analysed separately based on the mean ± SD for fascicle lengths, fascicle angles relative to the sagittal and the frontal planes, as well as the anatomical cross-sectional area (ASCA) and the volume of the muscles. Because the differences between the body sides were low, data from both sides were pooled for the final analysis, and are presented as mean ± SD as well as upper and lower quantiles (Q.25 and Q.75). Fascicle length was calculated by adding the lengths of the tendinous and fleshy parts of the respective fascicle. The ACSA and the volume of the muscles were calculated using convex envelopes of all fascicles of the same muscle. For this, virtual cross-sections at 1-mm intervals and perpendicular to the body's long axis were generated based on convex envelopes that surrounded all sectioned fascicles of a given muscle using 'Cloud2'. The ACSA of each virtual cross-section was determined and multiplied with its respective thickness (i.e. 1 mm) to determine the muscle volume. Note that the ACSA and the volume were determined from their origins to their insertions, with the exception of the PMN and PMJ, which were analysed only up to S1. To determine the fascicle angles relative to the frontal and the sagittal planes, we also used 'Cloud2'. The mean angle for each fascicle was calculated by first determining a series of angles along the fascicle (i.e. one value per millimetre) and then averaging these values. These mean fascicle angles were then compared with the data collected by Stokes & Gardner-Morse (1999) by aligning the two datasets based on vertebral levels. Note, we moved the Q from Stokes & Gardner-Morse by 4.5 cm and the PMJ + PMN by 2 cm cranial, in order to align these muscles in accordance to their origins and insertions. Then, Stokes & Gardner-Morse's raw data (i.e. the coordinates of the fascicle origins and insertions) were used to calculate mean fascicle angles in the same manner as in this study. To visualize the skeleton and the muscles, the open source program 'Pov Ray' (http://www.povray.org/) was used. For this, the 3D objects of the CT-scan and the 3D fascicles coordinates were combined and rendered with 'Pov-Ray' to obtain images from different views.

Results

Fascicle lengths

The lengths of the fleshy fascicle portions were comparable between the two medial dorsovertebral muscles (SP 5.9 ± 1.7 cm; M 6.6 ± 2.7 cm), as well as between the two lateral

Table 1 Mean ± SD of the lengths (cm) of the fleshy and tendinous fascicle parts for the following perivertebral muscles studied: SP, Spinalis thoracis; ILC, Iliocostalis lumborum; LG, Longissimus thoracis; M, Multifidus thoracis et lumborum; PMJ, Psoas major; PMN, Psoas minor; Q, Quadratus lumborum.

	Fleshy fascicle length (cm)		Tendinous fascicle length (cm)	
	Left side	Right side	Left side	Right side
SP	–	5.9 ± 1.7 (19)	–	7.7 ± 4.6 (15)
ILC	–	10.2 ± 3.4 (91)	–	6.3 ± 4.5 (56)
LG	–	9.6 ± 3.7 (133)	–	11.3 ± 9.2 (54)
M	–	6.6 ± 2.7 (75)	–	3.2 ± 1.5 (77)
PMJ	14.5 ± 2.9 (112)	14.6 ± 2.8 (87)	–	–
PMN	15.2 ± 1.8 (17)	8.5 ± 1.4 (9)	–	–
Q	5.5 ± 2.3 (101)	6.0 ± 2.1 (80)	3.3 ± 1.6 (88)	3.2 ± 1.4 (48)

Values in parentheses indicate the number of fascicles measured (for missing values, see methodological caveats). Note that the PMJ and the PMN were only analysed up to S1, therefore the distal tendinous parts were not measured.

ones (ILC 10.2 ± 3.4 cm; LG 9.6 ± 3.7 cm; Table 1). They were about half the length in the SP and M compared with those of the ILC and LG. With regards to the tendinous parts, the LG had the longest portions (11.3 ± 9.2 cm), while the M possessed the shortest of the epaxial muscles studied (3.2 ± 1.5 cm; Table 1).

In the ventrovertebral musculature, the fleshy fascicles were similar between PMJ and PMN (means for both sides: 14.6 ± 2.9 cm; 11.9 ± 1.6 cm; see Table 1 for values of each side), and thus longer than in any dorsovertebral muscle, while the Q had the shortest fleshy portions (mean for both sides: 5.8 ± 2.2 cm). The lengths of the tendinous portions could only be determined for Q (mean for both sides: 3.3 ± 1.5 cm), which was comparable to that of M.

ASCA and volume

Overall, the ACSA perivertebral musculature was largest in the mid-lumbar region (maxima: ILC at L2, LG at L3 and M at L4; Fig. 2). Among the dorsovertebral muscles, the LG had the greatest mean ACSA with 4.0 ± 3.0 cm^2 (pooled mean ± SD) compared with 1.9 ± 1.9 cm^2 for ILC and 1.4 ± 1.0 cm^2 for M. SP was the smallest muscle with 0.2 ± 0.1 cm^2 (Table 2). The ACSA of the ventrovertebral musculature was greatest at L3, and decreased nearly symmetrically in cranial and caudal directions (maximum for PMJ at L3 and PMN at L2; Fig. 2). The muscle with the greatest mean ACSA was PMJ with 3.9 ± 2.4 cm^2, followed by Q with 2.9 ± 1.3 cm^2 and PMN with 0.6 ± 0.5 cm^2 (Table 2).

Regarding muscle volume, the LG was the largest one among the dorsovertebral muscles with 186.7 ± 20.5 cm^3, compared with 80.1 ± 0.9 cm^3 for ILC, 46.5 ± 0.1 cm^3 for M and 4.9 ± 1.2 cm^3 for SP (Table 2). In the ventrovertebral musculature, PMJ was the largest muscle 101.5 ± 21.2 cm^3, followed by Q and PMN with 39.8 ± 12.0 cm^3 and 2.5 ± 3.4 cm^3, respectively (Table 2).

Fascicle angle

In the dorsovertebral muscles, fascicle angles relative to the sagittal plane ranged from 4.8 ± 4.4 ° in SP, over 6.5 ± 5.0 ° in LG, 10.9 ± 5.5 ° in ILC to 11.3 ± 6.4 ° in the M (pooled mean ± SD; Fig. 3a; see also Table 3), and from 3.8 ± 3.3 ° in SP, over 6.0 ± 6.1 ° in LG, 8.2 ± 5.2 ° in ILC to 13.7 ± 7.8 ° in M relative to the frontal plane (Fig. 3d; Table 3). As Fig. 3 illustrates, the fascicle angles were fairly similar among the dorsovertebral muscles when compared with the ventrovertebral muscles. Of the ventrovertebral muscles, the PMJ and the PMN were comparable to the dorsal muscles in having fascicle angles of 10.0 ± 4.6 ° and 5.2 ± 3.2 ° relative to the sagittal plane, whereas Q (27.9 ± 17.9 °) showed particularly high values of up to 90 ° near its origin (Table 3; Fig. 3b). In contrast to the sagittal angle, less variation occurred in the frontal angle, with values ranging from 20.0 ± 4.6 ° in PMN, 23.3 ± 6.8 ° in PMJ to 24.7 ± 11.1 ° in Q (Fig. 3). Along the thoracolumbar region, fascicle angles were less variable overall in the dorsal than in the ventral muscles, with only minor increases in the cranial and caudal muscle parts (Fig. 3a,d).

Discussion

Methodological caveats

Given the nature of the study, thorough selection of the donated body was critical for the quality of the data collected. Body donors are usually older than the population average, and therefore often show musculoskeletal pathologies and/or age-related degenerations and loss of muscle mass (Deyo & Tsui-Wu, 1987; Walsh et al. 1992; Schmidt et al. 2007). One limiting factor of the current study was the availability of a suitable donor. As discussed in detail below, the donated body in our study was average in his muscularity, compared with European men of his age

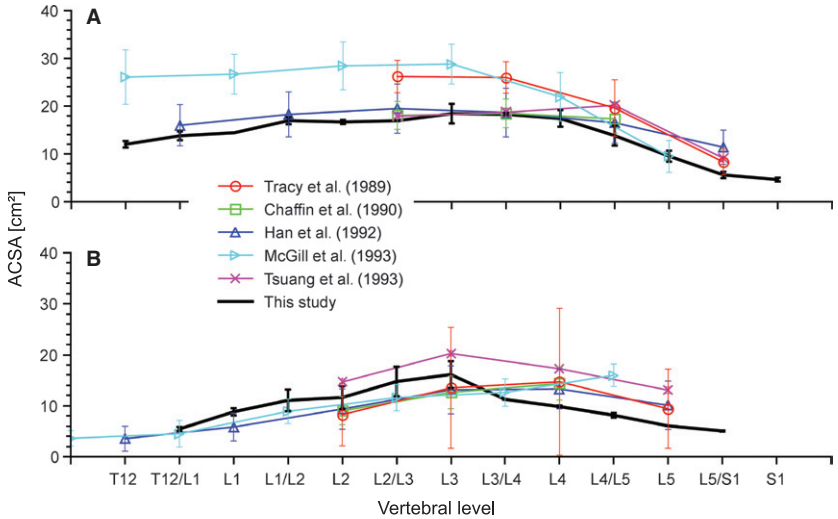

Fig. 2 Anatomical cross-sectional area (ACSA) of (a) the dorsovertebral (ILC + LG + M) and (b) the ventrovertebral muscles (PMN + PMJ + Q) in the thoracolumbar region from this study compared with results from previous studies.

Table 2 Mean ± SD of the ACSA (cm^2) and the volume (cm^3) of the perivertebral muscles across all vertebral levels studied (for muscle abbreviations, see Table 1).

	ACSA (cm^2)		Volume (cm^3)	
	Left side	Right side	Left side	Right side
SP	0.2 ± 0.1	0.2 ± 0.2	4.0	5.7
ILC	1.9 ± 2.1	1.8 ± 1.8	79.5	80.7
LG	4.3 ± 3.4	3.6 ± 2.6	201.1	172.2
M	1.5 ± 1.0	1.4 ± 1.0	46.4	46.6
PMJ	4.4 ± 2.5	3.3 ± 2.1	116.5	86.5
PMN	0.7 ± 0.6	0.6 ± 0.4	10.1	15.0
Q	3.3 ± 1.5	2.4 ± 0.9	48.3	31.3

Note that the muscle volumes were calculated from the anatomical cross-sectional areas of the virtual cross-sections and the distance at which they were determined (i.e. 1-mm intervals). ACSA, anatomical cross-sectional area.

(Fig. 2). He had no musculoskeletal degenerations or pathologies; except a slight scoliosis in the upper thoracic region, cranial to the back region studied.

Despite thorough fixation and positioning of the specimen (i.e. particular caution during the dissection was taken), small relative movements of the body were inevitable. For example, removal of the musculature on one side of the body leaves that particular side with less stability. Thus, slight bending of the specimen towards the undissected side occurred. This was detected and corrected using the reference markers. Nevertheless, the reconstruction of the dorsovertebral musculature was more precise as only the skin and the superficial back muscles had been removed at this time. Somewhat higher values were observed for the dissection of the ventrovertebral musculature due to the earlier removal of the dorsovertebral muscles and the abdominal wall (Fig. 1c). However, the error was low enough to still perform the measurements and to collect meaningful data.

Due to technical issues, not all data were collected for both sides of the body in this pilot study. For example, the left side served in establishing the data collection and processing, and no distinction was made between fleshy and tendinous fascicle parts. Therefore, a complete dataset was collected for the right side of the dorsovertebral muscles only. After completion of the data collection of the back, the torso was left relatively unstable, which hampered the data collection of the ventrovertebral muscles. For example, the right side (the last part dissected) was not included in the analyses of the fascicle angles because deformation of the Q impacted on the conformation of the PMN and the PMJ.

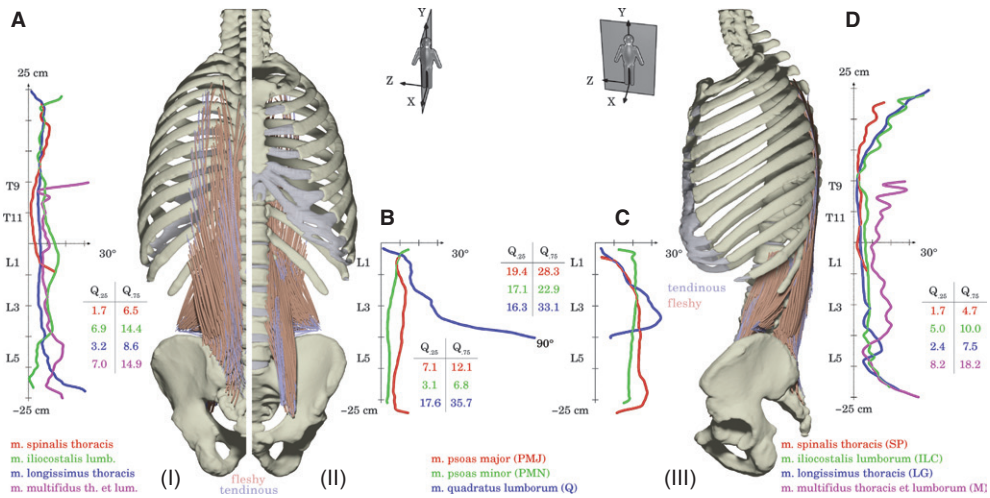

Fig. 3 3D reconstruction of the fascicles with their fleshy (red) and tendinous portions (blue) in (I) dorsal, (II) ventral and (III) lateral perspectives. Averaged angles of (a) and (d) the dorsovertebral and (b) and (c) the ventrovertebral fascicles relative to (a) and (b) the sagittal and (c) and (d) the frontal planes. Note the increase in angle towards the fascicle ends in the dorsovertebral muscles as well as very similar angle of the PMJ and the PMN compared with the Q.

Comparison with other data

The ACSAs determined for the dorsovertebral musculature in this study were generally consistent with data previously collected by Chaffin et al. (1990; CT: 96 women), Han et al. (1992; CT: four women, six men) and Tsuang et al. (1993; MRI: five men; Fig. 2a); although the former two studies investigated women, who were on average smaller and lighter than the donor studied herein (1.63 m vs. 1.72 m; 66.6 kg vs. 92.6 kg). In contrast, Tracy et al. (1989; MRI: 26 men) and McGill et al. (1993; MRI: 15 men) observed ACSAs almost twice the values of this study, but both studies investigated younger men (mean age 29 and 25.3 years, respectively, in contrast to our 57-year-old man). Comparison of the BMI (Frankenfield et al. 2001; Mensink et al. 2005) shows that our donor was obese (BMI: 31.3 kg m^{-2}, class I; WHO, Global database 2004), while the subjects of previous studies were normal (23.1 kg m^{-2}; Chaffin et al. 1990; Han et al. 1992; Tsuang et al. 1993; 25.0 kg m^{-2}; Tracy et al. 1989; McGill et al. 1993). Interestingly, the ACSAs of the ventrovertebral muscles (PMJ, PMN and Q) in our cadaver closely match the results from previous studies (except Tsuang et al. 1993; Fig. 2b), implying that ACSA may be less dependent on BMI, body mass or body height for the ventrovertebral musculature, but may be more closely related to these factors for the dorsovertebral musculature. However, compared with previous results, our values for the ventrovertebral muscles were slightly higher cranial and lower caudal to L3 (Fig. 2b). Thus, the PMN and PMJ were smaller, and the Q was larger in previous studies than in our donor.

Table 3 Mean ± SD of the fascicle angles (°) relative to the sagittal and the frontal planes (for missing values, see methodological caveats; for muscle abbreviations, see Table 1).

	Sagittal fascicle angles (°)		Frontal fascicle angles (°)	
	Left side	Right side	Left side	Right side
SP	4.3 ± 4.3	5.2 ± 4.4	3.1 ± 2.0	4.3 ± 4.0
ILC	10.6 ± 5.0	11.3 ± 5.9	8.6 ± 5.0	7.7 ± 5.3
LG	6.8 ± 5.2	6.0 ± 4.6	6.2 ± 6.1	5.8 ± 6.2
M	10.2 ± 5.8	12.3 ± 6.7	12.8 ± 7.5	14.5 ± 8.1
PMJ	10.0 ± 4.6	–	23.3 ± 6.8	–
PMN	5.2 ± 3.2	–	20.0 ± 4.6	–
Q	27.9 ± 17.9	–	24.7 ± 11.1	–

Regarding fascicle angles, we compared our data with those reported in Stokes & Gardner-Morse (1999; Fig. 4), who included data previously published by Macintosh & Bogduk (1991), Panjabi et al. (1991), Bogduk et al. (1992a,b) and Han et al. (1992). Note that these studies determined the muscle attachment sites in 3D as an approximation for their fibre orientation using x-ray images, combined with dissections (Macintosh & Bogduk, 1991; Bogduk et al. 1992a,b), a 3D digitizer (Panjabi et al. 1991) or CT images (Han et al. 1992). To compare these data with ours, we calculated the differences between the datasets (Fig. 4). Negative values indicate smaller angles observed in this study than in Stokes & Gardner-Morse (1999), while positive values indicate greater values observed herein. The biggest differences between the dorsovertebral data were found near the muscles' origins and insertions in the frontal plane (Fig. 4d), and around the thoracolumbar transition in the sagittal plane (only ILC; Fig. 4a). These differences are likely due to Stokes & Gardner-Morse's linear abstraction in the fascicles, i.e. not paying heed to the fascicle curvature near

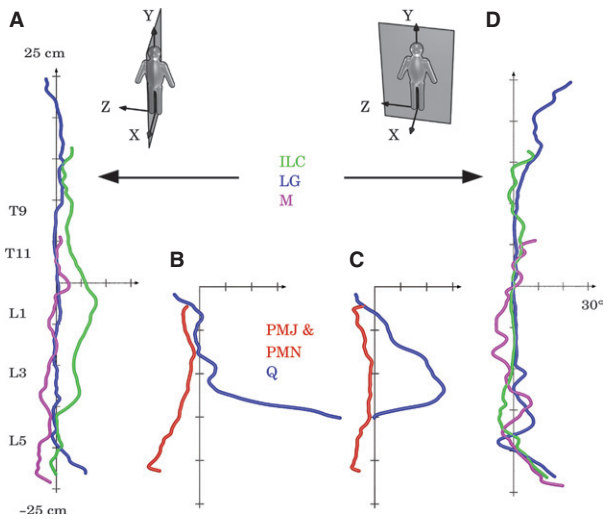

Fig. 4 Differences between the average fascicle angles of the dorsovertebral (a) and (d) and the ventrovertebral (b) and (c) fascicles relative to the sagittal (a) and (b) and the frontal planes (c) and (d) collected by Stokes & Gardner-Morse (1999) with the data collected in this study. Negative values indicate greater values in the former, positive values show greater angles in the latter study. Note that in this figure and in Fig. 3 the same dimensions of the axes were used.

the origins and insertions, as well as to the fascicle curvature due to the curved shape of the ILC. In contrast to the dorsovertebral muscles, for which the datasets were on the whole comparable, our values for the ventrovertebral musculature clearly differed from Stokes & Gardner-Morse's data. Particularly, the fascicle angles of Q, relative to the sagittal and the frontal planes, were much greater in the mid-lumbar and lower lumbar region in our donor (Fig. 4b,c). Furthermore, the comparison with previously published data on the M shows that our results are not only in agreement regarding the fascicle angles but also regarding the lengths of fleshy and tendinous fascicle portions (Rosatelli et al. 2008).

To summarize, our data are comparable with previous results for the dorsovertebral musculature, and thus the established method of a fascicle-wise dissection is suited in the collection of geometrical data for the intramuscular fascicle architecture of muscles. How much of the observed differences is the result of interspecific variability or due to different technical approaches remains open for future studies.

Functional consequences of muscle size and fascicle arrangement

Among the dorsovertebral muscles, the LG had the greatest volume (186.7 ± 20.5 cm^3), followed by the ILC (80.1 ± 0.9 cm^3) and the M (46.5 ± 0.2 cm^3). The SP was the smallest muscle with a volume of only 4.9 ± 1.2 cm^3 (Table 2). Consequently, the LG potentially produces the highest maximum contraction force (based on: force = cos angle*stress*volume/length; Lieber & Fridén, 2001), and thus is the strongest back muscle. Due to their relatively long fleshy fascicles and thus their relatively greater number of sarcomeres in series, the ILC and the LG can achieve greater shortening distances and produce a wider range of motion than the SP and the M. With its long tendinous fascicles, the LG may additionally be able to store more elastic energy than other epaxial muscles studied.

The M and the ILC had the greatest fascicle angles relative to the sagittal and the frontal planes. Higher angles favour the production of flexion and extension of the trunk, while lower angles contribute to its stabilization (Lieber & Fridén, 2001). Thus, the SP and the LG are overall architecturally better suited for stabilization. But note that the fascicle angles along with the whole muscle's geometry constantly change during motion and, with this, the instantaneous potential of torque production of the muscle. Therefore, the values reported herein only capture one specific architectural state.

Compared with the dorsovertebral muscles, the PMN and PMJ consistently show higher fascicle angles relative to the frontal plane, which is advantageous for the sagittal flexion they produce (Hansen et al. 2006). Additionally these muscles have sagittal fascicle angles that facilitate lateral bending of the trunk. Our PMJ data for the fascicle lengths compare well with the data reported by Bogduk and colleagues (Bogduk et al. 1992b; 14.6 ± 2.9 cm vs. 13.7 ± 1.4 cm). Confirming previous results (Phillips et al. 2008), the Q differed from all other muscles in having several architectural subunits defined by their distinct attachment sites and different fascicle lengths. Additionally, these muscles possess greater architectural variability between the body's left and right sides, and among specimens (Phillips et al. 2008; this study).

Outlook – muscle modelling

Our results provide a database, which aims at improving biomechanical models of the human trunk. Because the perivertebral muscles are represented by their fascicles, more detailed information can now be included in finite element mesh models. In these models, each muscle can be divided into subunits represented by specific mathematical formulas and parameters, which is essential for anisotropic muscle modelling (Vankan et al. 1996, 1998; Johansson et al. 2000; Jenkyn et al. 2002; Yucesoy et al. 2002; Oomens et al. 2003; Blemker et al. 2005). For example, different muscle properties for the tendinous and fleshy fascicle parts or different fibre types can now be incorporated. Further, properties such as stiffness, differing between the fascicle's longitudinal and transverse axes can be integrated. Such details will advance biomechanical modelling (Scott & Loeb, 1995; van Loocke et al. 2008; Azizi & Roberts, 2009; Morrow et al. 2010).

Acknowledgements

This study was generously supported by the Berufsgenossenschaft für Nahrungsmittel und Gastgewerbe (Erfurt, Germany), and we particularly thank R. Grieshaber and I. Bradl for their support. We also thank C. Anders, I. Bradl, M.S. Fischer, B. Hesse and C. Puta for very stimulating discussions and their continuing interest in our work. For his help with the CT-scans, we thank T. Schulz from the Institut für Diagnostische und Interventionelle Radiologie, Universitätsklinikum Jena (Germany). The titan-screws were kindly provided by R.D. Bader from the Gesichts- und Kieferchirugie, Universitätsklinikum Jena. Technical assistance by S. Müller, A. Wiegand, M. Szabó and S. Freund is gratefully acknowledged. We also thank L. Kruger for linguistically revising the manuscript.

References

Azizi E, Roberts TJ (2009) Biaxial strain and variable stiffness in aponeuroses. *J Physiol* **587**, 4309–4318.

Barr KP, Griggs M, Cadby T (2005) Lumbar stabilization: core concepts and current literature, Part 1. *Am J Phys Med Rehabil* **84**, 473–480.

Barr KP, Griggs M, Cadby T (2007) Lumbar stabilization: a review of core concepts and current literature, Part 2. *Am J Phys Med Rehabil* **86**, 72–80.

Benninghoff A, Rollhäuser H (1952) Zur inneren Mechanik des gefiederten Muskels [Interior mechanics of pennated muscles]. *Pflügers Arch* **254**, 527–548.

Blemker SS, Delp SL (2005) Three-dimensional representation of complex muscle architectures and geometries. *Ann Biomed Eng* **33**, 661–673.

Blemker SS, Delp SL (2006) Rectus femoris and vastus intermedius fiber excursions predicted by three-dimensional muscle models. *J Biomech* **39**, 1383–1391.

Blemker SS, Pinsky PM, Delp SL (2005) A 3D model of muscle reveals the causes of nonuniform strains in the biceps brachii. *J Biomech* **38**, 657–665.

Bogduk N, Macintosh JE, Pearcy MJ (1992a) A universal model of the lumbar back muscles in the upright position. *Spine* **17**, 897–913.

Bogduk N, Pearcy MJ, Hadfield G (1992b) Anatomy and biomechanics of psoas major. *Clin Biomech* **7**, 109–119.

Chaffin DB, Redfern MS, Erig M, et al. (1990) Lumbar muscle size and locations from CT scans of 96 women of age 40 to 63 years. *Clin Biomech* **5**, 9–16.

Chou R, Qaseem A, Snow V, et al. (2007) Diagnosis and treatment of low back pain: a joint clinical practice guideline from the American College of Physicians and the American Pain Society. *Ann Intern Med* **147**, 478–491.

Deyo RA, Tsui-Wu YJ (1987) Descriptive epidemiology of low-back pain and its related medical care in the United States. *Spine* **12**, 264–268.

Dumas GA, Poulin MJ, Roy B, et al. (1988) A three-dimensional digitization method to measure trunk muscle lines of action. *Spine* **13**, 532–541.

Dumas GA, Poulin MJ, Roy B, et al. (1991) Orientation and moment arms of some trunk muscles. *Spine* **16**, 293–303.

van Eijden TM, Koolstra JH, Brugman P (1996) Three-dimensional structure of the human temporalis muscle. *Anat Rec* **246**, 565–572.

Federative Committee on Anatomical Terminology (1998) *Terminologia Anatomica: International Anatomical Terminology*. Stuttgart: Georg Thieme.

Frankenfield DC, Rowe WA, Cooney RN, et al. (2001) Limits of body mass index to detect obesity and predict body composition. *Nutrition* **17**, 26–30.

Gans C (1982) Fiber architecture and muscle function. *Exerc Sport Sci Rev* **10**, 160–207.

Gans C, Bock WJ (1965) The functional significance of muscle architecture – a theoretical analysis. *Ergeb Anat Entwicklungsgesch* **38**, 115–142.

Han JS, Ahn JY, Goel VK, et al. (1992) CT-based geometric data of human spine musculature. Part I. Japanese patients with chronic low back pain. *J Spinal Disord* **5**, 448–458.

Hansen L, de Zee M, Rasmussen J, et al. (2006) Anatomy and biomechanics of the back muscles in the lumbar spine with reference to biomechanical modeling. *Spine* **31**, 1888–1899.

Jellema P, van Tulder MW, van Poppel MNM, et al. (2001) Lumbar supports for prevention and treatment of low back pain: a systematic review within the framework of the Cochrane Back Review Group. *Spine* **26**, 377–386.

Jenkyn TR, Koopman BHFJM, Huijing PA, et al. (2002) Finite element model of intramuscular pressure during isometric contraction of skeletal muscle. *Phys Med Biol* **47**, 4043–4061.

Johansson T, Meier P, Blickhan R (2000) A finite-element model for the mechanical analysis of skeletal muscles. *J Theor Biol* **206**, 131–149.

Kim SY, Boynton EL, Ravichandiran K, et al. (2007) Three-dimensional study of the musculotendinous architecture of supraspinatus and its functional correlations. *Clin Anat* **20**, 648–655.

Langenberg W (1970) Morphologie, physiologischer Querschnitt und Kraft des M. erector spinae im Lumbalbereich des Menschen [Morphology, physiological cross-section and strength of the M. erector spinae in the lumbar region of man]. *Z Anat ntwicklungsgesch* **132**, 158–190.

Lemos RR, Epstein M, Herzog W, et al. (2004) A framework for structured modeling of skeletal muscle. *Comput Methods Biomech Biomed Eng* **7**, 305–317.

Lemos RR, Rokne J, Baranoski GVG, et al. (2005) Modeling and simulating the deformation of human skeletal muscle based on anatomy and physiology. *Comput Animat Virtual Worlds* **16**, 319–330.

Lieber RL, Fridén J (2001) Clinical significance of skeletal muscle architecture. *Clin Orthop Relat Res* **23**, 140–151.

Linton SJ, van Tulder MW (2001) Preventive interventions for back and neck pain problems: what is the evidence? *Spine* **26**, 778–787.

van Loocke M, Lyons CG, Simms CK (2008) Viscoelastic properties of passive skeletal muscle in compression: stress-relaxation behaviour and constitutive modelling. *J Biomech* **41**, 1555–1566.

Macintosh JE, Bogduk N (1991) The attachments of the lumbar erector spinae. *Spine* **16**, 783–792.

McGill SM, Santaguida L, Stevens J (1993) Measurement of the trunk musculature from T5 to L5 using MRI scans of 15 young males corrected for muscle fibre orientation. *Clin Biomech* **8**, 171–178.

Mensink GBM, Lampert T, Bergmann E (2005) Übergewicht und Adipositas in Deutschland 1984–2003 [Overweight and obesity in Germany 1984–2003]. *Bundesgesundheitsblatt Gesundheitsforschung Gesundheitsschutz* **48**, 1348–1356.

Morrow DA, Haut Donahue TL, Odegard GM, et al. (2010) Transversely isotropic tensile material properties of skeletal muscle tissue. *J Mech Behav Biomed Mater* **3**, 124–129.

Oomens CWJ, Maenhout M, van Oijen CH, et al. (2003) Finite element modelling of contracting skeletal muscle. *Philos Trans R Soc Lond B Biol Sci* **358**, 1453–1460.

Panjabi MM, Takata K, Goel VK, et al. (1991) Thoracic human vertebrae. Quantitative three-dimensional anatomy. *Spine* **16**, 888–901.

Paul AC (2001) Muscle length affects the architecture and pattern of innervation differently in leg muscles of mouse, guinea pig, and rabbit compared to those of human and monkey muscles. *Anat Rec* **262**, 301–309.

Phillips S, Mercer S, Bogduk N (2008) Anatomy and biomechanics of quadratus lumborum. *Proc Inst Mech Eng [H]* **222**, 151–159.

Poelstra KA, Eijkelkamp MF, Veldhuizen AG (2000) The geometry of the human paraspinal muscles with the aid of three-dimensional computed tomography scans and 3-Space Isotrak. *Spine* **25**, 2176–2179.

Rosatelli AL, Ravichandiran K, Agur AM (2008) Three-dimensional study of the musculotendinous architecture of lumbar multifidus and its functional implications. *Clin Anat* **21**, 539–546.

Sacks RD, Roy RR (1982) Architecture of the hind limb muscles of cats: functional significance. *J Morphol* **173**, 185–195.

Schmidt CO, Raspe H, Pfingsten M, et al. (2007) Back pain in the German adult population: prevalence, severity, and sociodemographic correlates in a multiregional survey. *Spine* **32**, 2005–2011.

Scott SH, Loeb GE (1995) Mechanical properties of aponeurosis and tendon of the cat soleus muscle during whole-muscle isometric contractions. *J Morphol* **224**, 73–86.

Stark H, Schilling N (2010) A novel method of studying fascicle architecture in relaxed and contracted muscles. *J Biomech* **43**, 2897–2903.

Stokes IAF, Gardner-Morse M (1999) Quantitative anatomy of the lumbar musculature. *J Biomech* **32**, 311–316.

Tracy MF, Gibson MJ, Szypryt EP, et al. (1989) The geometry of the muscles of the lumbar spine determined by magnetic resonance imaging. *Spine* **14**, 186–193.

Tsuang YH, Novak GJ, Schipplein OD, et al. (1993) Trunk muscle geometry and centroid location when twisting. *J Biomech* **26**, 537–546.

van Tulder MW, Jellema P, van Poppel MNM, et al. (2006) WITHDRAWN: lumbar supports for prevention and treatment of low-back pain. *Cochrane Database Syst Rev (Online)* **2**, CD001823. doi:10.1002/14651858.CD001823.pub2.

Vankan WJ, Huyghe JM, Janssen JD, et al. (1996) A 3-D finite element model of blood perfused rat gastrocnemius medialis muscle. *Eur J Morphol* **34**, 19–24.

Vankan WJ, Huyghe JM, van Donkelaar CC, et al. (1998) Mechanical blood-tissue interaction in contracting muscles: a model study. *J Biomech* **31**, 401–409.

Walsh K, Cruddas M, Coggon D (1992) Low back pain in eight areas of Britain. *J Epidemiol Community Health* **46**, 227–230.

Wu G, Cavanagh PR (1995) ISB recommendations for standardization in the reporting of kinematic data. *J Biomech* **28**, 1257–1261.

Wu G, Siegler S, Allard P, et al. (2002) ISB recommendation on definitions of joint coordinate system of various joints for the reporting of human joint motion–part I: ankle, hip, and spine. International Society of Biomechanics. *J Biomech* **35**, 543–548.

Yucesoy CA, Koopman BHFJM, Huijing PA, et al. (2002) Three-dimensional finite element modeling of skeletal muscle using a two-domain approach: linked fiber-matrix mesh model. *J Biomech* **35**, 1253–1262.

Supporting Information

Additional Supporting Information may be found in the online version of this article:

Data S1. Dataset of the reconstructed muscle fascicles of the Spinalis thoracis (right side) as zip-file. Each zip-file contains a muscle (m) and tendon (t) data set. The data files contain the coordinates of the vertex points (x #tab y #tab z) of all fascicles, which are separated by an empty line.

Data S2. Dataset of the reconstructed muscle fascicles of the Iliocostalis lumborum (right side) as zip-file. For details, see Data S1.

Data S3. Dataset of the reconstructed muscle fascicles of the Longissimus thoracis (right side) as zip-file. For details, see Data S1.

Data S4. Dataset of the reconstructed muscle fascicles of the Multifidus thoracis et lumborum (right side) as zip-file. For details, see Data S1.

Data S5. Dataset of the reconstructed muscle fascicles of the Psoas major (left side) as zip-file. For details, see Data S1.

Data S6. Dataset of the reconstructed muscle fascicles of the Psoas minor (left side) as zip-file. For details, see Data S1.

Data S7. Dataset of the reconstructed muscle fascicles of the Quadratus lumborum (left side) as zip-file. For details, see Data S1.